Available online at www.sciencedirect.com
ScienceDirect
Carbohydrate Research 342 (2007) 597–609
Carbohydrate RESEARCH

Comparative ^{1}H NMR and molecular modeling study of hydroxy protons of β-D-Gal*p*-(1→4)-β-D-Glc*p*NAc-(1→2)-α-D-Man*p*-(1→O)$(CH_2)_7CH_3$ analogues in aqueous solution

Philippe F. Rohfritsch,[a] Martin Frank,[a] Corine Sandström,[b] Lennart Kenne,[b] Johannes F. G. Vliegenthart[a] and Johannis P. Kamerling[a,*]

[a]*Bijvoet Center, Department of Bio-Organic Chemistry, Utrecht University, Padualaan 8, NL-3584 CH Utrecht, The Netherlands*
[b]*Department of Chemistry, Swedish University of Agricultural Sciences, PO Box 7015, SE-750 07 Uppsala, Sweden*

Received 19 May 2006; accepted 7 July 2006
Available online 17 August 2006

Dedicated to the memory of Professor Nikolay K. Kochetkov

Abstract—The ^{1}H chemical shifts, coupling constants, temperature coefficients, exchange rates, and inter-residual ROEs have been measured, in aqueous solution, for the hydroxy and amine/amide proton resonances of a set of β-D-Gal*p*-(1→4)-β-D-Glc*p*NAc-(1→2)-α-D-Man*p*-(1→O)$(CH_2)_7CH_3$ analogues. From the structural data, a few significant structural features could be ascertained, such as a preferential *anti*-conformation for the amide protons of the *N*-acetyl and *N*-propionyl groups. The introduction of systematic modifications at Gal 2-C and Gal 6-C resulted in alterations of the Gal 4-OH, Gal 3-OH, and GlcNAc 3-OH areas, since variations in chemical shifts and temperature coefficient were observed. In order to verify the possibility of hydrogen bonds, molecular dynamics simulations in the gas phase and explicit solvent were performed and correlated with the experimental data. A network of hydrogen bonds to solvent molecules was observed, but no strong intramolecular hydrogen bonding was observed.

Keywords: Hydroxy protons; ^{1}H NMR; Synthetic analogues; LacNAc-Man; Molecular dynamics simulation

1. Introduction

In recent years, the consideration of hydroxy protons in the conformational analysis of carbohydrates by ^{1}H NMR spectroscopy has shown to be a valuable addition to the study of the carbon-bound ring and exocyclic protons. The assignment of the resonances of the carbon-bound protons is quite often hampered by several factors: (i) the relatively narrow dispersion of their chemical shifts (3.0–4.5 ppm) leading to overlapping signals; (ii) the limited number of inter-residual distance constraints obtained from NOE-type experiments (nuclear Overhauser effect) observable in D_2O; (iii) the frequently high flexibility of oligosaccharides generating ensembles of conformers in solution. Taking into account the importance of hydrogen bond interactions in carbohydrates,[1,2] the use of the exchangeable hydroxy protons in H_2O in conformational studies has given new insights into the 3D structure of carbohydrates in solution. Typical ^{1}H NMR examples comprise the conformational analysis of polysaccharides,[3–8] synthetic and isolated oligosaccharides,[9–17] and glycopeptides.[18–20] To obtain structural information in terms of stereochemistry, inter-proton distances, hydrogen bonding, and hydration, hydroxy protons are usually studied at low temperatures in a solvent mixture of 85% H_2O and 15% deuterated acetone.[12] Such conditions, derived from the 'water in supercooling conditions',[11,21,22] are applied to reduce the rate of exchange with water. They are used in association with the pulse

* Corresponding author. Tel.: +31 30 253 34 79; fax: +31 30 254 09 80; e-mail: j.p.kamerling@chem.uu.nl

0008-6215/$ - see front matter © 2006 Elsevier Ltd. All rights reserved.
doi:10.1016/j.carres.2006.07.003

sequences that efficiently suppress the water signal without affecting the resonances of the exchangeable protons.

Recently, we have investigated the substrate specificity of four different recombinant sialyltransferases, namely, two α-2,3-sialyltransferases (rST3Gal III and hST3Gal IV) and two α-2,6-sialyltransferases (hST6Gal I and hST6Gal II), toward synthetic β-D-Gal*p*-(1→4)-β-D-Glc*p*NAc-(1→2)-α-D-Man*p*-(1→O)$(CH_2)_7CH_3$ **1** and a set of 11 synthetic trisaccharide analogues **2**–**12** (Fig. 1), carrying modifications at Gal 2-C or 6-C, in addition to an alternative *N*-acyl group at GlcNAc 2-C.[23] It turned out that replacing the *N*-acetyl group of GlcNAc by an *N*-propionyl group increased the catalytic activity (V_{max}) of both ST3Gal and ST6Gal (ST3Gal, α-2,3-sialyltransferase for galactose; ST6Gal, α-2,6-sialyltransferase for galactose). In addition, both ST6Gal's show a greater tolerance toward modified substrates, as they are active on both Gal and GalNAc terminal residues.[23]

Here, we present chemical shifts (δ), chemical shift differences ($\Delta\delta$) between **1** and the methyl glycosides of the three constituents, chemical shift differences ($\Delta\delta'$) between **1** and **2**–**12**, temperature coefficients $d\delta/dT$, vicinal coupling constants $^3J_{OH,CH}$ or $^3J_{NH,CH}$, rates of exchange with water K_{ex}, and ROEs (rotational nuclear Overhauser effect) for the hydroxy and amide protons of **1**–**12**. Furthermore, we performed molecular dynamics simulations in the gas phase and explicit solvent to study the stability of the intramolecular hydrogen bonding network and the influence of solvation.

2. Results

2.1. Assignment of hydroxy and amide proton resonances

The structures of β-D-Gal*p*-(1→4)-β-D-Glc*p*NAc-(1→2)-α-D-Man*p*-(1→O)$(CH_2)_7CH_3$ **1**, derived from glycoprotein N-glycans containing type II chains, and of its analogues **2**–**12**, are summarized in Figure 1. Hydroxyl functions of the terminal Gal residue were modified at 2-C (**3**–**4**, OH→H; **5**–**6**, OH→NHAc; **7**–**8**, OH→NHPr) or at 6-C (**9**–**10**, OH→H; **11**–**12**, OH→NH_2), and the *N*-acyl function of the subterminal GlcNAc unit in half of the structures was replaced by an *N*-propionyl group (**2**, **4**, **6**, **8**, **10**, **12**). ^{1}H NMR spectra were recorded for the samples in 85% H_2O/15% $(CD_3)_2CO$ at pH ~ 7 for **1**–**10**, and at pH ~ 6.4 for **11**–**12**. The selected pH values made it possible to observe all hydroxy protons. Measurements were carried out at 268 K, a temperature low enough to slow down the exchange of the OH protons with the solvent. Making use of the scalar connectivities between OH and ring/exocyclic protons, proton assignments were obtained from two-dimensional (2D) DQF-COSY (double quantum filtered-correlated spectroscopy) and TOCSY (total scalar correlation spectroscopy measurements). As a typical example, the 2D DQF-COSY and TOCSY spectra of **2** are depicted in Figure 2. In Tables 1–3, the OH/NH ^{1}H chemical shifts (δ, ppm) of the monosaccharide constituents, the chemical shift differences $\Delta\delta$ between **1** and β-D-Gal*p*-OMe,

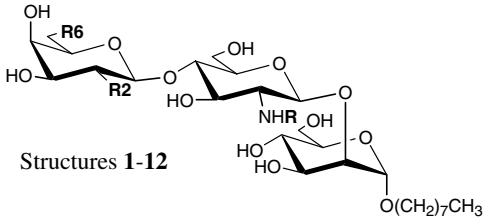

Structures **1**-**12**

	Structure	R	R2	R6
1	β-Gal-β-GlcNAc-α-Man-octyl	Ac	OH	OH
2	β-Gal-β-GlcNPr-α-Man-octyl	Pr	OH	OH
3	2-deoxy-β-Gal-β-GlcNAc-α-Man-octyl	Ac	H	OH
4	2-deoxy-β-Gal-β-GlcNPr-α-Man-octyl	Pr	H	OH
5	2-acetamido-2-deoxy-β-Gal-β-GlcNAc-α-Man-octyl	Ac	NHAc	OH
6	2-acetamido-2-deoxy-β-Gal-β-GlcNPr-α-Man-octyl	Pr	NHAc	OH
7	2-deoxy-2-propionamido-β-Gal-β-GlcNAc-α-Man-octyl	Ac	NHPr	OH
8	2-deoxy-2-propionamido-β-Gal-β-GlcNPr-α-Man-octyl	Pr	NHPr	OH
9	6-deoxy-β-Gal-β-GlcNAc-α-Man-octyl	Ac	OH	H
10	6-deoxy-β-Gal-β-GlcNPr-α-Man-octyl	Pr	OH	H
11	6-amino-6-deoxy-β-Gal-β-GlcNAc-α-Man-octyl	Ac	OH	NH_2
12	6-amino-6-deoxy-β-Gal-β-GlcNPr-α-Man-octyl	Pr	OH	NH_2

Figure 1. Structures of synthetic trisaccharide octyl glycosides **1**–**12** used in this study.

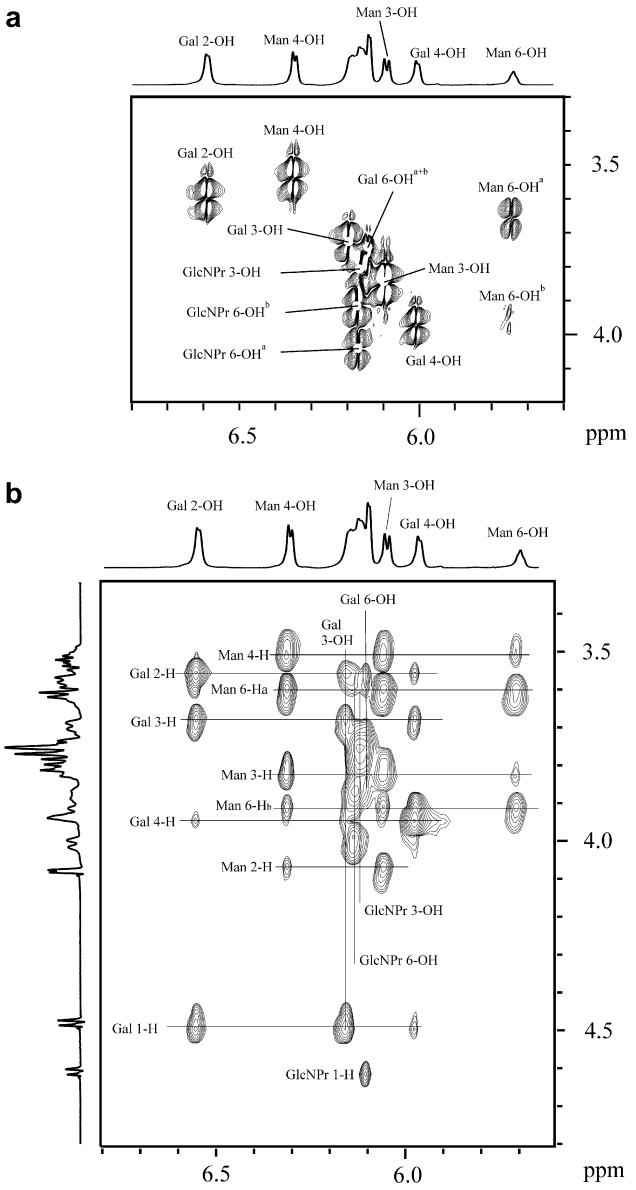

Figure 2. 2D DQF-COSY (a) and 2D TOCSY (b) ^{1}H NMR spectra at 268 K of β-D-Gal*p*-(1→4)-β-D-Glc*p*NPr-(1→2)-α-D-Man*p*-(1→O)$(CH_2)_7CH_3$ (**2**). The ^{1}H NMR data for the ring protons were previously reported.[24]

β-D-Glc*p*NAc-OMe, or α-D-Man*p*-OMe, and the chemical shift differences $\Delta\delta'$ between **1** and **2**–**12** are presented. The OH/NH ^{1}H NMR data of the reference monosaccharide methyl glycosides have been reported earlier.[13,14,19] The $\Delta\delta$ values give insight into the difference in chemical environment of the OH/NH protons when present in monosaccharides or as constituent in trisaccharides, whereas the $\Delta\delta'$ values reflect the effect of systematic modifications on the hydration of hydroxy and amine/amide protons in the modified trisaccharide structures. Additionally, the tables include temperature coefficients $d\delta/dT$, vicinal coupling constants $^{3}J_{OH,CH}$ or $^{3}J_{NH,CH}$, and rates of exchange with water K_{ex}, for the OH/NH protons of the Gal constituent (Table 1) for nonmodified Gal (**1**–**2**), 2-deoxy-Gal (Gal^{2d} in **3**–**4**), GalNAc (Gal^{2NAc} in **5**–**6**), GalNPr (Gal^{2NPr} in **7**–**8**), 6-deoxy-Gal (Gal^{6d} in **9**–**10**), and 6-amino-Gal (Gal^{6NH_2} in **11**–**12**), as well as for hydroxy and amide protons of GlcNAc/GlcNPr (Table 2), and hydroxy protons of Man (Table 3), respectively.

2.2. Chemical shifts δ and chemical shift differences $\Delta\delta$ and $\Delta\delta'$

To illustrate the resolution of the hydroxy proton resonances, the NH and OH regions of the ^{1}H NMR spectra of β-D-Gal*p*-(1→4)-β-D-Glc*p*NAc-(1→2)-α-D-Man*p*-(1→O)$(CH_2)_7CH_3$ **1**, and of some Glc*p*NPr analogues with terminal Gal (**2**), 2-deoxy-Gal (**4**), GalNPr (**8**), and 6-deoxy-Gal (**10**) are shown in Figure 3.

Comparison of the chemical shifts of the OH/NH signals of **1** with those of the three methyl glycosides, β-D-Gal*p*-OMe, β-D-Glc*p*NAc-OMe, and α-D-Man*p*-OMe, shows some remarkably large $\Delta\delta$ values (Tables 1–3). The 2-OH, 3-OH, 4-OH, and 6-OH resonances of the terminal Gal unit in **1** showed somewhat higher δ_{OH} values than the corresponding signals from β-D-Gal*p*-OMe, reflecting a slightly higher deshielding; the $\Delta\delta$ values amount +0.09, +0.14, +0.14, and +0.05, respectively (Table 1). Comparing the $\delta_{OH/NH}$ values of β-D-Glc*p*NAc-OMe with those of the internal (1→4)-linked GlcNAc residue in **1** demonstrated a strong shielding effect on GlcNAc 3-OH ($\Delta\delta$ −0.23 ppm), and minor effects on GlcNAc 2-NH ($\Delta\delta$ +0.08 ppm) and 6-OH ($\Delta\delta$ +0.13 ppm) (Table 2). The shielding of 3-OH is due to the presence of a Gal residue on GlcNAc 4-O that might restrain the interactions between GlcNAc 3-OH and the solvent. Positioning of the 3-OH proton in close proximity to the Gal ring and the glycosidic O has been found to provide a shielding effect.[15] In lactose and compounds with similar stereochemistry and conformation around the glycosidic linkage, such a close proximity renders possibly the formation of a hydrogen bond between Gal 5-O and Glc 3-OH.[22] The effects observed for GlcNAc 2-NH and GlcNAc 6-OH are weaker. Finally, compared with Man 6-OH of α-D-Man*p*-OMe, the Man 6-OH signal of the reducing end Man unit in **1** showed an upfield shift of −0.17 ppm, whereas for Man 3-OH and 4-OH, the $\Delta\delta$ values were +0.05 and +0.08, respectively (Table 3). The shielding of Man 6-OH in **1** might be attributed to the spatial proximity of the *N*-acetyl group of GlcNAc. This shielding is slightly increased in the case of N-propionylated structures **2**, **4**, **6**, **8**, **10**, and **12**, as reflected by higher $\Delta\delta$ values than in the corresponding N-acetylated structures.

The conversion of Gal into Gal^{2d} (**1**→**3** or **4**) obviously affects the Gal 4-OH environment as is evident from $\Delta\delta'$ values of around −0.20 ppm (Table 1). This is a remarkable feature since Gal 2-H and Gal 4-OH

Table 1. ^{1}H NMR chemical shifts (δ in ppm), chemical shift differences ($\Delta\delta$) between **1** and β-D-Gal*p*-OMe, chemical shift differences ($\Delta\delta'$) between **1** and **2**–**12**, temperature coefficients (dδ/dT in ppb deg^{-1}), $^3J_{OH,CH}$ or $^3J_{NH,CH}$ coupling constants (J in hertz), and exchange rates (K_{ex} in s^{-1}) for the different hydroxy and amine/amide protons of the (modified) Gal residue in compounds **1**–**12** (Fig. 1)

	OH/NH (**5**–**8**) protons at Gal 2-C					OH protons at Gal 3-C				
	δ	$\Delta\delta$ or $\Delta\delta'$	dδ/dT	J	K_{ex}	δ	$\Delta\delta$ or $\Delta\delta'$	dδ/dT	J	K_{ex}
1	6.57	0.09[a]	−11.1	n.d.	n.d.	6.18	0.14[a]	n.d.	n.d.	n.d.
2	6.55	−0.02	−11.5	5.0	n.d.	6.15	−0.03	−11.1	5.5	n.d.
3	—	—	—	—	—	6.17	−0.01	−11.7	n.d.	n.d.
4	—	—	—	—	—	6.16	−0.02	−11.4	n.d.	n.d.
5	8.58	[b]	−8.6	9.7	n.d.	6.20	[b]	−11.6	n.d.	n.d.
6	8.59	[b]	−8.5	9.7	n.d.	6.21	[b]	n.d.	n.d.	n.d.
7	8.46	[b]	−8.7	9.7	n.d.	6.10	[b]	−10.8	6.8	n.d.
8	8.46	[b]	−8.6	9.7	n.d.	6.14	[b]	−10.9	7.0	n.d.
9	6.53	−0.04	−11.5	5.5	27	6.09	−0.09	−10.9	4.6	32
10	6.53	−0.04	−11.6	5.3	27	6.11	−0.07	−11.0	5.1	32
11	6.62	0.05	−12.1	5.0	n.d.	6.29	0.11	−11.2	n.d.	n.d.
12	6.62	0.05	−11.6	4.8	n.d.	6.29	0.11	−10.0	n.d.	n.d.

	OH protons at Gal 4-C					OH protons at Gal 6-C				
	δ	$\Delta\delta$ or $\Delta\delta'$	dδ/dT	J	K_{ex}	δ	$\Delta\delta$ or $\Delta\delta'$	dδ/dT	J	K_{ex}
1	5.99	0.14[a]	−11.4	4.4	n.d.	6.13	0.05[a]	n.d.	n.d.	n.d.
2	5.97	−0.02	−10.8	5.5	n.d.	6.12	−0.01	−12.0	4.8	n.d.
3	5.80	−0.19	−12.0	4.6	60	6.09	−0.04	−14.9	n.d.	43
4	5.78	−0.21	−8.3	5.5	133	6.09	−0.04	−12.1	n.d.	53
5	6.08	[b]	n.d.	n.d.	n.d.	6.09	[b]	n.d.	n.d.	n.d.
6	6.08	[b]	−11.5	5.3	n.d.	6.10	[b]	−14.9	n.d.	n.d.
7	6.06	[b]	−11.9	5.7	n.d.	6.11	[b]	−13.5	5.3	n.d.
8	6.05	[b]	−12.9	n.d.	n.d.	6.11	[b]	−12.5	4.2	n.d.
9	5.98	−0.01	−11.7	5.3	n.d.	—	—	—	—	—
10	5.98	−0.01	−11.8	4.5	n.d.	—	—	—	—	—
11	6.30	0.31	n.d.	n.d.	n.d.	—	—	—	—	—
12	6.30	0.31	n.d.	n.d.	n.d.	—	—	—	—	—

n.d.: Could not be determined due to spectral overlap (K_{ex} and dδ/dT) or poorly resolved signals ($^3J_{OH,CH}$ or $^3J_{NH,CH}$).
[a] $\Delta\delta$ was determined by comparison with reference β-D-Gal*p*-OMe.[13,14]
[b] Not calculated since Gal (**1**) and GalNAc/GalNPr (**5**–**8**) should not be directly compared.

Table 2. ^{1}H NMR chemical shifts (δ in ppm), chemical shift differences ($\Delta\delta$) between **1** and β-D-Glc*p*NAc-OMe, chemical shift differences ($\Delta\delta'$) between **1** and **2**–**12**, temperature coefficients (dδ/dT in ppb deg^{-1}), $^3J_{OH,CH}$ or $^3J_{NH,CH}$ coupling constants (J in hertz), and exchange rates (K_{ex} in s^{-1}) for the hydroxy and amine protons of the GlcNAc/GlcNPr residue in compounds **1**–**12** (Fig. 1)

	NH protons at GlcNAc/GlcNPr 2-C				OH protons at GlcNAc/GlcNPr 3-C					OH protons at GlcNAc/GlcNPr 6-C				
	δ	$\Delta\delta$ or $\Delta\delta'$	dδ/dT	J	δ	$\Delta\delta$ or $\Delta\delta'$	dδ/dT	J	K_{ex}	δ	$\Delta\delta$ or $\Delta\delta'$	dδ/dT	J	K_{ex}
1	8.50	0.08[a]	−7.8	9.2	6.17	−0.23[a]	n.d.	n.d.	n.d.	6.12	0.13[a]	n.d.	n.d.	n.d.
2	8.37	−0.13	−7.9	9.5	6.10	−0.07	−12.2	3.7	n.d.	6.13	0.01	−11.6	5.8	n.d.
3	8.51	0.01	−7.7	9.7	6.27	0.10	−12.6	3.1	21	6.14	0.02	−10.7	n.d.	33
4	8.38	−0.12	−7.7	9.5	6.21	0.04	−11.8	3.3	33	6.16	0.04	−11.5	n.d.	n.d.
5	8.50	0	−8.1	7.7	6.07	−0.10	n.d.	n.d.	n.d.	6.17	0.05	−12.3	n.d.	n.d.
6	8.37	−0.13	−8.1	8.6	6.04	−0.13	−10.9	n.d.	n.d.	6.19	0.07	−11.5	n.d.	n.d.
7	8.50	0	−7.7	8.6	6.10	−0.07	−11.0	n.d.	n.d.	6.17	0.05	−12.7	5.3	n.d.
8	8.37	−0.13	−8.0	9.2	6.06	−0.11	−11.1	n.d.	n.d.	6.19	0.07	−13.2	5.9	n.d.
9	8.51	0.01	−7.8	9.4	5.88	−0.29	−8.2	n.d.	n.d.	6.10	−0.02	−12.5	5.5	n.d.
10	8.39	−0.11	−8.1	9.5	5.86	−0.31	−8.2	n.d.	n.d.	6.13	0.01	−12.5	5.1	n.d.
11	8.53	0.03	−7.6	9.5	6.65	0.48	n.d.	n.d.	n.d.	6.13	0.01	−11.8	n.d.	n.d.
12	8.40	−0.10	−7.9	9.7	6.60	0.43	n.d.	n.d.	n.d.	6.16	0.04	−12.0	n.d.	n.d.

n.d.: Could not be determined due to spectral overlap (K_{ex} and dδ/dT) or poorly resolved signals ($^3J_{OH,CH}$ or $^3J_{NH,CH}$).
[a] $\Delta\delta$ was determined by comparison with reference β-D-Glc*p*NAc-OMe.[13,14,19]

are not very close in space. The conversion of Gal into Gal[6d] (**1**→**9** or **10**) has only a small influence on Gal 3-OH ($\Delta\delta'$ −0.08 ppm). On the other hand, when the Gal 6-C hydroxy group is replaced by an amino function

Table 3. ^{1}H NMR chemical shifts (δ in ppm), chemical shift differences ($\Delta\delta$) between **1** and α-D-Man*p*-OMe, chemical shift differences ($\Delta\delta'$) between **1** and **2**–**12**, temperature coefficients ($d\delta/dT$ in ppb deg^{-1}), $^{3}J_{OH,CH}$ coupling constants (J in hertz), and exchange rates (K_{ex} in s^{-1}) for the hydroxy protons of the Man residue in compounds **1**–**12** (Fig. 1)

	OH protons at Man 3-C					OH protons at Man 4-C					OH protons at Man 6-C				
	δ	$\Delta\delta$ or $\Delta\delta'$	$d\delta/dT$	J	K_{ex}	δ	$\Delta\delta$ or $\Delta\delta'$	$d\delta/dT$	J	K_{ex}	δ	$\Delta\delta$ or $\Delta\delta'$	$d\delta/dT$	J	K_{ex}
1	6.10	0.05[a]	−14.4	7.2	n.d.	6.34	0.08[a]	−11.7	5.9	n.d.	5.76	−0.17[a]	−13.5	n.d.	n.d.
2	6.05	−0.05	−15.3	7.7	n.d.	6.31	−0.03	−11.9	5.9	n.d.	5.70	−0.06	−14.2	5.0	n.d.
3	6.07	−0.03	−14.8	n.d.	n.d.	6.32	−0.02	−11.7	5.5	31	5.75	−0.01	−13.9	3.5	83
4	6.05	−0.05	−14.3	6.9	74	6.31	−0.03	−11.7	5.9	32	5.70	−0.06	−13.9	4.3	n.d.
5	6.09	−0.01	n.d.	n.d.	n.d.	6.32	−0.02	−12.0	5.9	n.d.	5.75	−0.01	−14.0	n.d.	n.d.
6	6.09	−0.01	−15.9	n.d.	n.d.	6.31	−0.03	−11.8	n.d.	n.d.	5.72	−0.04	−13.9	n.d.	n.d.
7	6.09	−0.01	−12.2	7.3	n.d.	6.31	−0.03	−11.7	n.d.	n.d.	5.74	−0.02	−13.6	5.3	n.d.
8	6.07	−0.03	−12.8	7.5	n.d.	6.30	−0.04	−12.0	5.3	n.d.	5.69	−0.07	−14.4	5.3	n.d.
9	6.06	−0.04	−14.8	7.7	n.d.	6.31	−0.03	−11.9	5.3	23	5.73	−0.03	−13.7	5.5	n.d.
10	6.06	−0.04	−15.0	7.7	n.d.	6.31	−0.03	−11.6	5.5	22	5.71	−0.05	−14.1	4.8	n.d.
11	6.14	0.04	−15.6	n.d.	n.d.	6.33	−0.01	−11.7	5.7	n.d.	5.78	0.02	n.d.	n.d.	n.d.
12	6.13	0.03	−15.5	7.7	n.d.	6.33	−0.01	−11.6	n.d.	n.d.	5.75	−0.01	−14.0	n.d.	n.d.

n.d.: Could not be determined due to spectral overlap (K_{ex} and $d\delta/dT$) or poorly resolved signals ($^{3}J_{OH,CH}$).
[a] $\Delta\delta$ was determined by comparison with reference α-D-Man*p*-OMe.[13,14]

(Gal → Gal^{6NH_2}; **1**→**11** or **12**), Gal 3-OH and Gal 4-OH are deshielded by +0.11 and +0.31 ppm, respectively. These downfield shifts might be attributed to the deshielding effect of the positive charge of the NH_3^+ group, since the value of $\Delta\delta'$ reflects the distance from the charged group.

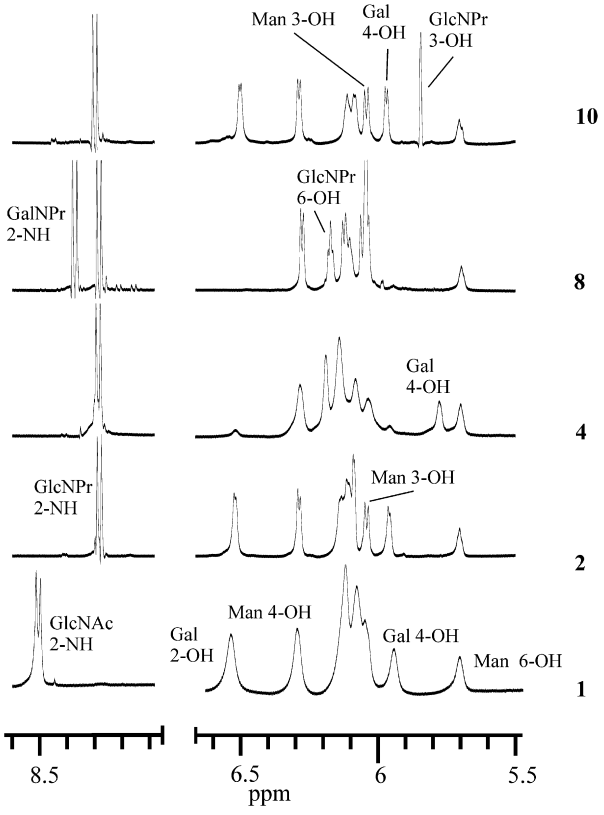

Figure 3. Resolution-enhanced 600 MHz 1D ^{1}H NMR spectra obtained at 268 K of the hydroxy and amide proton regions of β-D-Gal*p*-(1→4)-β-D-Glc*p*NAc-(1→2)-α-D-Man*p*-(1→O)$(CH_2)_7CH_3$ (**1**) and its analogues **2** (GlcNAc→GlcNPr), **4** (Gal→Gal^{2d}, GlcNAc→GlcNPr), **8** (Gal→Gal^{NPr}, GlcNAc→GlcNPr), and **10** (Gal→Gal^{6d}, GlcNAc→GlcNPr).

The GlcNAc 6-OH chemical shifts were very similar in **1**–**12** (Table 2). The persistent shift of GlcNAc 2-NH from ~8.51 to ~8.38 ppm, when replacing the *N*-acetyl group (**1**, **3**, **5**, **7**, **9**, and **11**) by an *N*-propionyl group (**2**, **4**, **6**, **8**, **10**, and **12**), reflects the increased steric hindrance of the hydration of the more bulky and more hydrophobic *N*-propionyl group. Compared with **1**, the chemical shift of GlcNAc/GlcNPr 3-OH is seriously affected by structural changes at Gal 6-C. When replacing Gal by Gal^{6d} (**9**–**10**), a large upfield shift is observed for GlcNAc/GlcNPr 3-OH ($\Delta\delta' \sim -0.30$ ppm). As mentioned above, an upfield shift can reflect a reduced hydration. In comparison to 3-OH in **1**, such a reduced hydration might either be due to a closer proximity to 5-O of Gal as a result of a change in the glycosidic conformation occurring upon substitution of Gal 6-OH by Gal 6-H, or to a significant modification of the solvation shells caused by the hydrophobic methyl group in Gal^{6d}. On the other hand, the large downfield shift in the GlcNAc/GlcNPr 3-OH ($\Delta\delta'$ ca. +0.45 ppm) resonance, when Gal is replaced by Gal^{6NH_2} (**11**–**12**), may indicate (i) a change in the interresidual hydrogen bond network; (ii) the existence of a transient hydrogen bonding between GlcNAc 3-OH and Gal 6-NH; (iii) modifications in the nearby water structure; or (iv) an influence of the positive charge. Per pair of compounds (**1**–**2**, **3**–**4**, etc.), replacing the *N*-acetyl group by an *N*-propionyl group causes very small upfield shifts for GlcNAc/GlcNPr 3-OH (ca. 0.03 ppm).

Comparison of the Man 3-OH, Man 4-OH, and Man 6-OH signals of **1** with those of **2**–**12** shows only small $\Delta\delta'$ values (Table 3), indicating that the structural modifications in the Gal and GlcNAc units of **1** have no influence on the hydration or hydrogen bonding properties of the Man residue. Notably, the Man 6-OH

protons resonate systematically at somewhat higher δ values for the GlcNAc units than for the GlcNPr units.

2.3. Temperature coefficients dδ/dT

The temperature dependency of chemical shifts of hydroxy protons can clearly be seen in compounds **1**–**12**. As an example, the OH/NH proton regions of **10** at different temperatures between 265 and 273 K are depicted in Figure 4. Going from lower to higher temperature, a clear line broadening is observed for most of the OH signals. Generally, low absolute temperature coefficients (about -3 ppb deg^{-1}) are correlated with strong hydrogen bonds.[9] For **1**–**12**, all hydroxy protons, except for three, have dδ/d$T < -10$ ppb deg^{-1} (Tables 1–3), illustrating that strong interactions do not occur for this series. It has been noticed earlier that amide protons have lower temperature coefficients than hydroxy protons.[19,20] The dδ/dT values of Gal^{NAc}/Gal^{NPr} 2-NH in **5**–**8** (Table 1) and of GlcNAc/GlcNPr 2-NH in **1**–**12** (Table 2), confirm this finding (dδ/dT around -8 ppb deg^{-1}). Interestingly, the three exceptions mentioned above, Gal^{2d} 4-OH in **4** (Table 1) and GlcNAc/GlcNPr 3-OH in **9** and **10** (Table 2), have also dδ/dT around -8 ppb deg^{-1}, which can be indicative of the involvement in weak hydrogen bonds, when associated with K_{ex} and $\Delta\delta'$ variations.

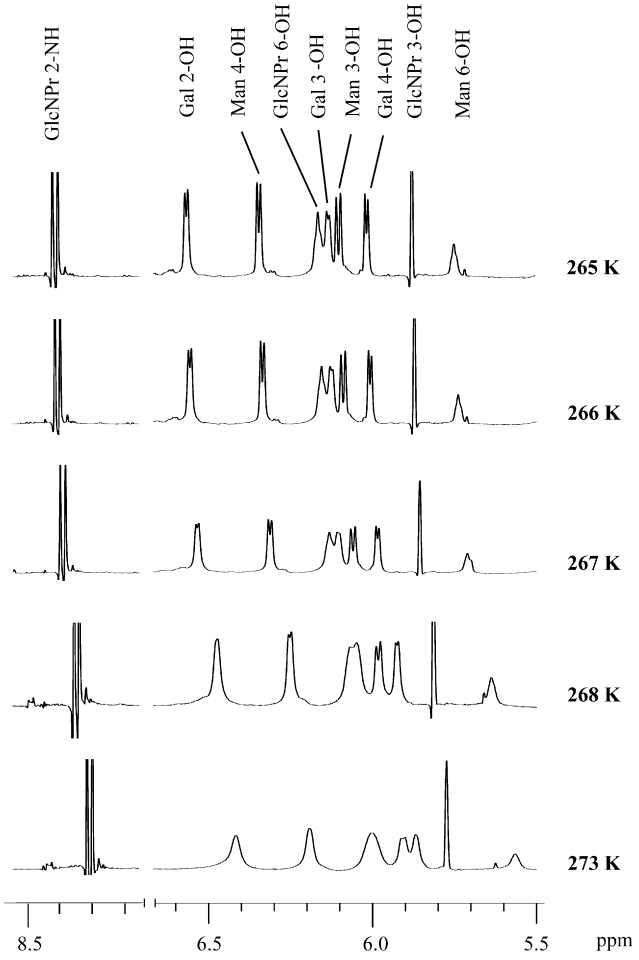

Figure 4. Resolution-enhanced 600 MHz 1D ^{1}H NMR spectra of the hydroxy and amide proton regions of 6-deoxy-β-D-Gal*p*-(1→4)-β-D-Glc*p*NPr-(1→2)-α-D-Man*p*-(1→O)(CH$_2$)$_7$CH$_3$ (**10**) at different temperatures ranging from 273 to 265 K.

2.4. Vicinal coupling constants $^3J_{OH,CH}$ and $^3J_{NH,CH}$

From the Karplus equation[25] applied to hydroxy protons, a free rotation around the C–O bond is reflected by vicinal coupling constants ($^3J_{OH,CH}$) of about 5.5 ± 1 Hz. The higher values indicate a preference (about 70%) for an *anti*-conformation of the H–C–O–H structural element.[26] Such a behavior is observed for all Man 3-OH protons ($^3J_{OH,CH}$ 6.9–7.7 Hz; Table 3). Here, the proximity of a GlcNAc or GlcNPr unit (1→2)-linked to the adjacent Man residue may restrain the free rotation, and forces Man 3-OH protons to adopt this *anti*-conformation. In the monosaccharide methyl glycoside where no rotational restrictions occur, 3-OH of Man has a $^3J_{OH,CH}$-value of 5 Hz. The *N*-propionyl group at 2-C seems also to constrain the motion allowed for Gal^{NPr} 3-OH protons in **7** and **8** (Gal^{NPr}; $^3J_{OH,CH} \sim 6.9$ Hz; Table 1). Lower $^3J_{OH,CH}$ values reflect a *syn*-conformation of the H–C–O–H structural element, suggesting a restricted rotation that can be associated with the involvement in hydrogen bonding interaction as observed for Glc 3-OH of lactose[22] or GlcNAc 3-OH of *N*,*N*′-diacetyl-chitobiose.[19] Typical examples are seen for GlcNAc/GlcNPr 3-OH in **2**–**4** (Table 2). For the 3-OH of GlcNAc/GlcNPr in the other compounds, $^3J_{OH,CH}$ could not be measured, due to the small linewidths that suggested values below 3 Hz (Figs. 3 and 4).

anti-Conformations have also been reported for amide functions.[13,18–20] Indeed, all GlcNAc/GlcNPr 2-NH signals show large $^3J_{NH,CH}$ values (**1**–**4** and **6**–**12**, 8.6–9.7 Hz; **5**, 7.7 Hz; Table 2), as well as the Gal^{NAc}/Gal^{NPr} 2-NH signals in **5**–**8** (9.7 Hz; Table 1).

2.5. Rates of exchange with the solvent K_{ex}

Strong signal overlapping in the 2D NOE/EXSY spectra of **1**–**12** at 268 K, hampered accurate determination of exchange rates for most compounds. Only some signals in **3**–**4** (Gal→Gal^{2d}) and **9**–**10** (Gal→Gal^{6d}) generated exchange rate values (Tables 1–3). The high K_{ex} values observed for Gal^{2d} 4-OH in **3**–**4**, Man 3-OH in **4**, and Man 6-OH in **3**, reflect significant accessibility to the solvent, and thus likely an outermost location on the molecule. On the other hand, low K_{ex} values (Man 4-OH in **3**–**4** and **9**–**10**; Gal^{2d} 6-OH, GlcNAc/GlcNPr 3-OH in **3**–**4**; GlcNAc 6-OH in **3**; Gal^{6d} 2-OH, and Gal^{6d} 3-OH in **9**–**10**) indicate limited exchange with the solvent that

may originate either from the presence of hydrogen bonds[14,15] or from the proximity with some nearby bulky groups,[19] which limits the access to the solvent. However, since only very few K_{ex} values could be calculated, no solid conclusions can be drawn from these data.

2.6. ROESY experiments

Though space interactions can be detected by NOESY (nuclear Overhauser effect correlation spectroscopy) experiments, but discrimination between signals from chemical exchange and from dipolar relaxation can only be achieved via ROESY experiments (rotating-frame exchange spectroscopy). ROE cross-peaks originating from chemical exchange have the same sign as the diagonal peaks, while cross-peaks originating from dipolar relaxation have the opposite sign. In Table 4, the interresidual and long-distance intraresidual (more than three covalent bonds) cross-peaks, specific to ROESY spectra, are listed for Gal variants and GlcNAc/GlcNPr of the β-D-Gal*p*-(1→4)-β-D-Glc*p*NAc-(1→2)-α-D-Man*p*-(1→O)$(CH_2)_7CH_3$ analogues (**1**–**12**). Only ROEs originating from dipolar relaxation, and not from chemical exchange, were detected. None of the hydroxy protons of the Man residue gives ROE cross-peaks.

Intraresidual ROEs between GlcNAc/GlcNPr 2-NH and GlcNAc/GlcNPr 1-H were observed for **1**–**10**. For **5**–**8** (replacement of Gal by Gal^{NAc} or Gal^{NPr}), intraresidual ROEs were detected between Gal^{NAc}/Gal^{NPr} 2-NH and Gal^{NAc}/Gal^{NPr} 1-H. When N-acetylated, GlcNAc 2-NH (**1**, **3**, **5**, **7**, **9**, **11**) or Gal^{NAc} 2-NH (**5**–**6**) showed ROE cross-peaks with methyl protons of the *N*-acetyl groups. In a similar way, with N-propionylated GlcNPr 2-NH (**2**, **4**, **6**, **8**, **10**, **12**) or Gal^{NPr} 2-NH (**7**–**8**), ROE cross-peaks were formed with the methylene and methyl protons of the *N*-propionyl group.

Interresidual ROEs were observed between Gal/Gal^{NAc}/Gal^{NPr}/Gal^{6d} 1-H (**2**, **6**–**10**) and GlcNAc/GlcNPr 3-OH, suggesting a spatial proximity of these protons regardless of the modifications introduced in the analogues. The structures in which Gal has been replaced by Gal^{6d} (**9**–**10**) or Gal^{6NH_2} (**11**–**12**) showed cross-peaks between GlcNAc/GlcNPr 6-OH and Gal^{6d}/Gal^{6NH_2} 2-H, and for **2** and **9**–**11** between Gal/Gal^{6d}/Gal^{6NH_2} 2-OH and GlcNAc/GlcNPr 6-H.

Table 4. Inter and long distance intraresidual ROEs observed with OH and NH protons for Gal variants and GlcNAc/GlcNPr of β-D-Gal*p*-(1→4)-β-D-Glc*p*NAc-(1→2)-α-D-Man*p*-(1→O)$(CH_2)_7CH_3$ analogues (**1**–**12**). Cross-peaks from less than three covalent bonds and detected by TOCSY experiments are not reported

	Gal residue and its variants in **3**–**12**		GlcNAc/GlcNPr		
	OH protons at 3-C	OH/NH protons at 2-C	OH protons at 6-C	OH protons at 3-C	NH protons at 2-C
1					Ac CH_3
					GlcNAc 1-H
2		Gal 1-H		GlcNPr 1-H	Pr CH_2
		GlcNPr 6-H		Gal 1-H	Pr CH_3
					GlcNPr 1-H
3					Ac CH_3
					GlcNAc 1-H
4					Pr CH_2
					Pr CH_3
					GlcNPr 1-H
5	GalNAc 1-H	Ac CH_3			Ac CH_3
		GalNAc 1-H			GlcNAc 1-H
6		Ac CH_3		GalNAc 1-H	Pr CH_2
		GalNAc 1-H			Pr CH_3
					GlcNPr 1-H
7		Pr CH_2		GalNPr 1-H	Ac CH_3
		Pr CH_3			GlcNAc 1-H
		GalNPr 1-H			
8		Pr CH_2		GalNPr 1-H	Pr CH_2
		Pr CH_3		Pr CH_2	Pr CH_3
		GalNPr 1-H			GlcNPr 1-H
9	GlcNAc 6-H	GlcNAc 6-H	6-Deoxy-Gal 2-H	6-Deoxy-Gal 1-H	Ac CH_3
				GlcNAc 2-H	GlcNAc 1-H
10		GlcNPr 6-H	6-Deoxy-Gal 2-H	6-Deoxy-Gal 1-H	Pr CH_2
					Pr CH_3
					GlcNPr 1-H
11		GlcNAc 6-H	6-Amino-Gal 2-H		Ac CH_3
12			6-Amino-Gal 2-H		Pr CH_2
					Pr CH_3

No cross-peaks were detected for Man 3-OH, Man 4-OH or Man 6-OH.

2.7. Molecular dynamics simulation

In order to gain deeper insight into the three-dimensional structure and the ability of the molecules to form intramolecular hydrogen bonds, molecular dynamics (MD) simulations of the trisaccharide fragments contained in **1**, **3**, **9**, and **11** have been performed in gas phase and in solvent. Solvation was accounted either by the implicit generalized born/surface area (GB/SA) model[27] or by the TIP3 water model using periodic boundary conditions. Even if intramolecular hydrogen bonding is overemphasized when no explicit solvent is present, gas phase or GB/SA simulations of appropriate length (in the nanosecond range) can give an overview of the possible intramolecular hydrogen bonds. Such simulations do not represent the situation in solvated systems, but give information on the hydrogen bonds that the systems can possibly form.

Two 30 ns MD simulations of **1** using AMBER* at 300 K revealed two frequently occurring hydrogen bonds: GlcNAc(3-OH)-Gal(5-O) (90%) and Man-(3-OH)-GlcNAc(5-O) (55%) (Fig. 5a). Two weaker interresidual hydrogen bonds between GlcNAc(3-OH)-Gal(6-OH) (30%) and GlcNAc(6-OH)-Gal(2-OH) (20%) (Fig. 5a) are predicted, but practically disappear when a continuum solvent model is included in the simulation. Using the GB/SA model, all hydrogen bonds probabilities decrease (Fig. 5b). When using an explicit solvent during the simulation, most of the intramolecular hydrogen bonds vanish (<1%) (Fig. 5c). As expected, the two previously highly populated hydrogen bonds see their probability significantly reduced, dropping from 90% to 33% for GlcNAc(3-OH)-Gal(5-O) and from 55% to 7% for Man(3-OH)-GlcNAc(5-O). Instead of forming intramolecular hydrogen bonds with the ring atoms of the adjacent residue, the GlcNAc 3-OH and Man 3-OH groups are now predominantly forming hydrogen bonds with the solvent molecules. It can be shown that both ring and glycosidic O are significantly less exposed to the solvent.

From autocorrelation analysis, the lifetimes of the GlcNAc(3-OH)-Gal(5-O) and Man(3-OH)-GlcNAc-(5-O) hydrogen bonds have been estimated to be about 7 ps. This number has to be taken with care since the estimation of the lifetime is very sensitive to the sampling interval and criterion used for the existence of a hydrogen bond. GB/SA simulations of compounds **3**, **9**, and **11** reveal no significant differences in the orientation of the glycosidic bonds (Fig. 6). In compound **9**, a hydrogen bond between Gal 2-OH and GlcNAc 6-OH occurred for about 20% of the time. In compound **11**, in contrast to the other compounds, the hydrogen bond between GlcNAc 3-OH and Gal 5-O is significantly reduced (about 35% in contrast to 70% for **9**). The NH_3^+ group of **11** forms a hydrogen bond to Gal 4-OH (65%) and, to a lesser extent, to GlcNAc 3-OH (17%). Compound **3** behaves in a very similar way to **1**. However, several transitions to the *anti* ϕ conformation of the β(1→4) linkage are observed, meaning that replacing the 2-OH group with an H atom lowers the transition barrier of the ϕ torsion.

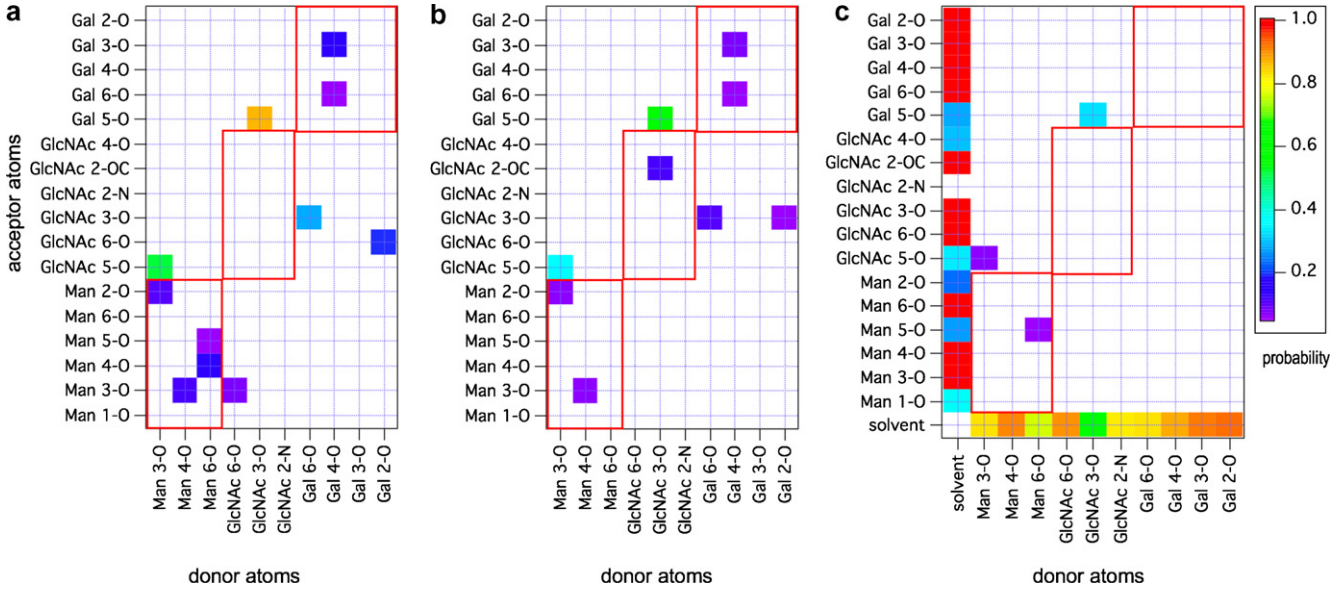

Figure 5. Analysis of intramolecular hydrogen bonds and interactions in gas phase (a), using a continuum solvent model (GB/SA) (b), and in explicit solvent (c) on compound **1**. The geometric criterions required for hydrogen bonding are: H-acceptor distance <2.5 Å and donor–H–acceptor angle >120°. Only hydrogen bonds that occur >5% were considered. Two interresidual H bonds displayed a population higher than 5%: GlcNAc(3-OH)-Gal(5-O) and Man(3-OH)-GlcNAc(5-O) (7%) (percent values in explicit solvent). The areas inside the red rectangles correspond to intraresidual H bonds.

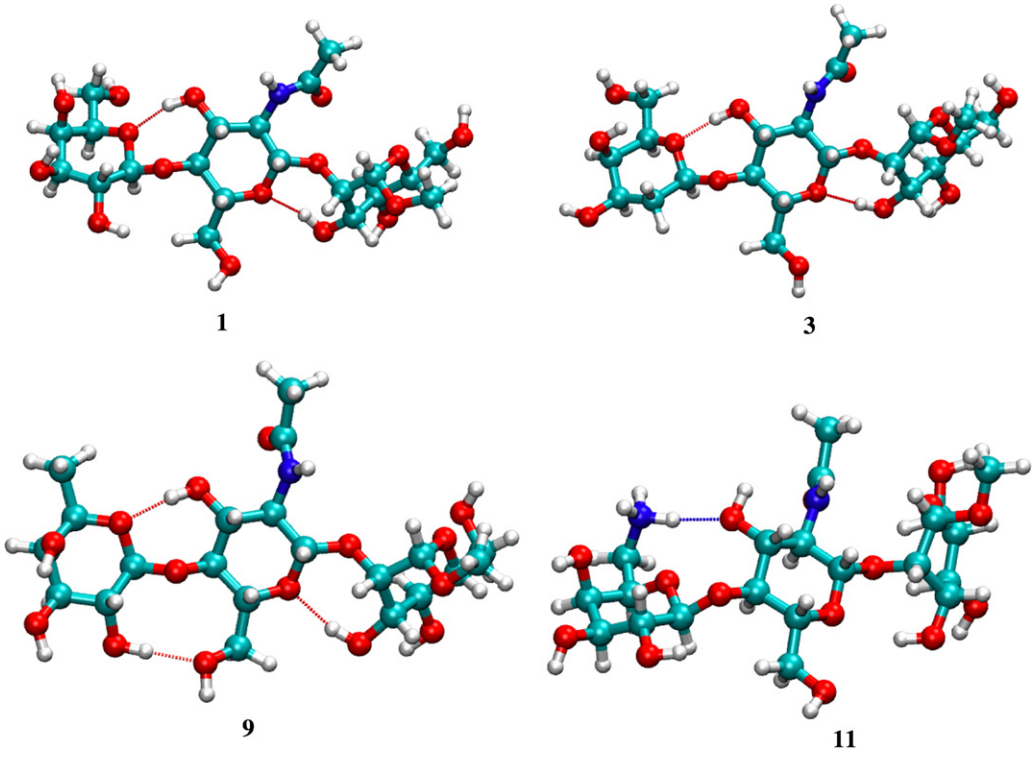

Figure 6. Examples of interresidual hydrogen bonds for GB/SA simulations of **1**, **3**, **9**, and **11**.

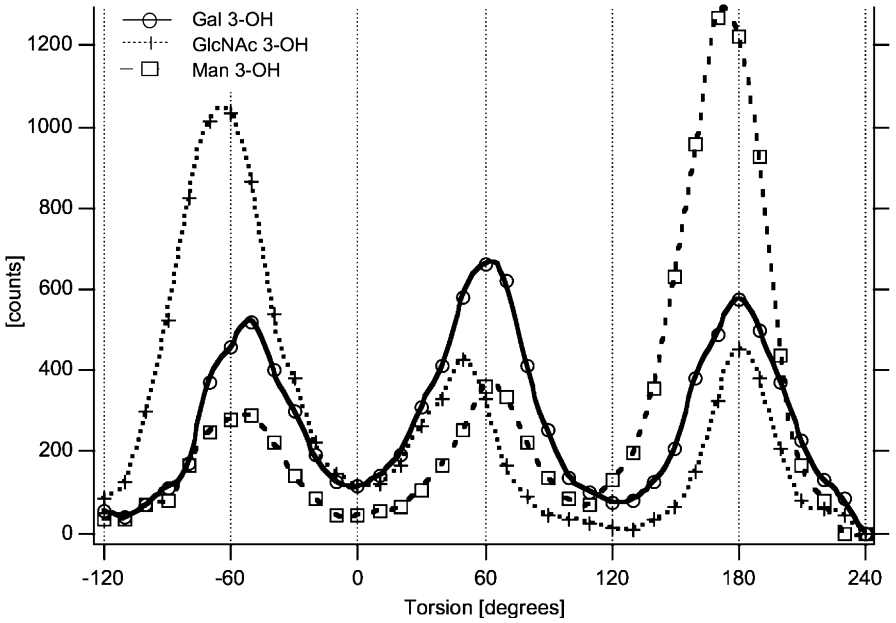

Figure 7. Histograms of the H–C–O–H torsions derived from the MD simulations in explicit solvent. The Gal 3-OH group shows no preference in orientation, whereas GlcNAc 3-OH preferably adopts a *gauche* (−60°) and Man 3-OH a *trans* (180°) orientation.

As experimental proof for the existence of hydrogen bonds, temperature coefficients, exchange rates, or unusual $^{3}J_{OH,CH}$ values are generally used. Exemplified for the 3-OH groups, a histogram of the H–C–O–H torsions derived from the solvent simulations, is shown in Figure 7. The torsion values for Gal 3-OH are evenly distributed between the three staggered orientations and should result in $^{3}J_{OH,CH}$ values around 5.5 Hz. For GlcNAc 3-OH, a *gauche* preference is observed and should lead to a smaller coupling constant. For Man 3-OH, the

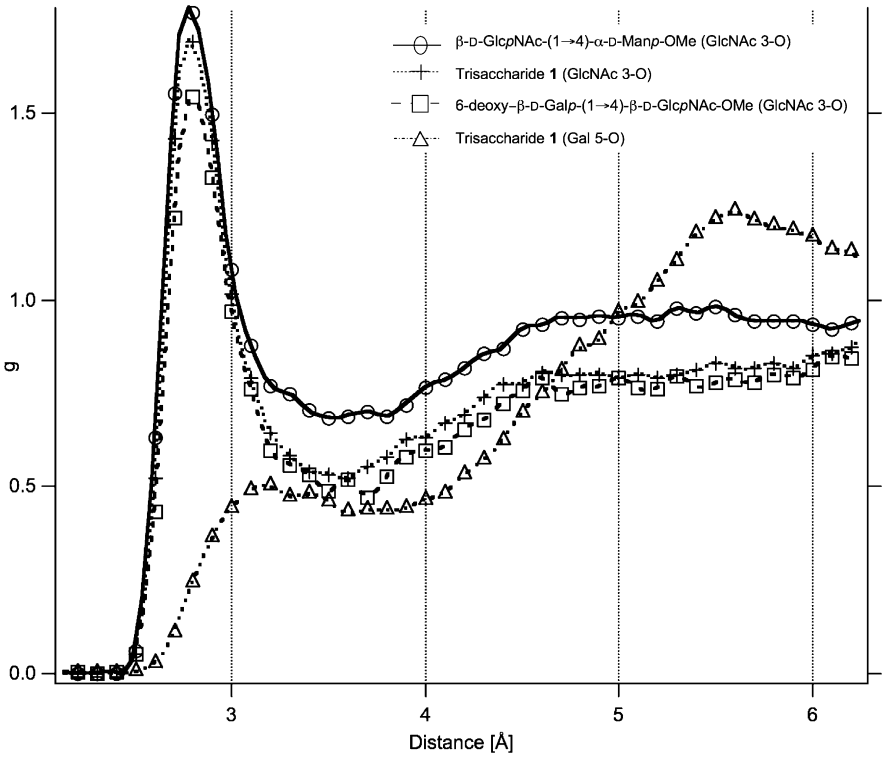

Figure 8. Radial distribution (rdf) of water molecules in the vicinity of GlcNAc 3-OH. The solvent density in the second solvation shell is significantly reduced when β-D-Gal*p* is linked at position GlcNAc 4-O. Highly ordered water in the first solvation shell is still present as shown by the intense peak at 2.7 Å. Reduction of the Gal 6-OH group has some effect on the solvent shell of GlcNAc 3-OH. For comparison, the rdf for Gal 5-O is included.

trans orientation has the highest population, resulting in an increased $^{3}J_{OH,CH}$ value. These predictions derived from the MD simulations, are in excellent agreement with the experimental values (Tables 1–3).

The influence of the substitution on the solvation of the GlcNAc 3-OH group has been investigated by comparing MD simulations of trisaccharide **1** with simulations of the corresponding β-D-Glc*p*NAc-(1→2)-α-D-Man*p*-OMe and 6-deoxy-β-D-Gal*p*-(1→2)-β-D-Glc*p*NAc-OMe disaccharides. To measure the extent of solvent ordering near GlcNAc 3-OH, radial distribution functions have been calculated for these compounds using the GlcNAc 3-O atom as coordinate center (Fig. 8). The disaccharide β-D-Glc*p*NAc-(1→2)-α-D-Man*p*-OMe served as a reference. Connecting a monosaccharide to position 4-C of GlcNAc (compound **1** GlcNAc 3-OH in Fig. 8) slightly decreases the water density in the first solvation shell (until 3.4 Å). The average number of water molecules, determined from integration of the curve, drops from 3.0 to 2.5 only. In the second solvation shell (between 3.4 and 4.5 Å), the water density around GlcNAc 3-OH is more pronouncedly reduced in the intact trisaccharide **1** as well as in the 6-deoxy-β-D-Gal*p*-(1→2)-β-D-Glc*p*NAc-OMe disaccharide (Fig. 8). Remarkably, a significant ordering is still present in the first solvation shell of all compounds. This can possibly originate from tightly bound water molecules on the surface of the carbohydrate molecule close to the GlcNAc 3-OH group. For comparison, the radial distribution function of Gal 5-O in **1** shows a completely different pattern (compound **1** (Gal 5-O) in Fig. 8).

3. Discussion

In this study, the hydroxy proton resonances of a set of synthetic type II trisaccharides modified at 2-C or 6-C of the terminal Gal unit and at 2-C of the subterminal GlcNAc residue[24] were investigated. Structural data including chemical shifts, vicinal coupling constants, temperature coefficients, rates of exchange with the solvent, and ROEs are reported for the Gal, GlcNAc, and Man units of the β-D-Gal*p*-(1→4)-β-D-Glc*p*NAc-(1→2)-α-D-Man*p*-(1→O)$(CH_2)_7CH_3$ variants **1**–**12**, as well as results derived from molecular dynamics simulations performed on compounds **1**, **3**, **9**, and **11**.

For all structures, GlcNAc/GlcNPr 2-NH shows a preferential *anti*-conformation and has intraresidual ROEs with either CH_3 protons of *N*-acetyl groups (**1**, **3**, **5**, **7**, **9**, **11**) or CH_2 and CH_3 protons of *N*-propionyl groups (**2**, **4**, **6**, **8**, **10**, **12**), as well as with GlcNAc/GlcNPr 1-H. Similar results are found for the β-D-Gal*p*-(1→4)-β-D-Glc*p*NAc-based analogues **5**–**8**, wherein Gal^{NAc}/Gal^{NPr} 2-NH shows an *anti*-conformation

and ROE cross-peaks with either CH_3 (**5**–**6**) or CH_2–CH_3 (**7**–**8**) protons of the *N*-acyl groups. Previously, it has been shown for a ^{13}C-enriched *N*-acetyllactosamine disaccharide,[21] that GlcNAc 3-OH and Gal 1-H, as well as GlcNAc 6-H and Gal 2-OH are close enough (<3 Å) to generate cross-peaks in ROESY experiments. The occurrence of ROE cross-peaks between Gal/Gal^{6d}/Gal^{6NH_2} 2-OH and GlcNAc/GlcNPr 6-H for **1**–**2** and **9**–**11** is in good agreement with the average structure found in the MD simulations. The hydroxymethyl group remains mainly in the *gg* or *gt* conformation and no hydrogen bond between 6-OH and 2-OH is formed in this orientation. Since ROEs between GlcNAc 6-OH and Gal^{6d}/Gal^{6NH_2} 2-H (**9**–**12**) could be detected, as well as lower K_{ex} values for Gal^{6d} 2-OH in **9** and **10**, the occurrence of a weak hydrogen bond between the Gal 2-OH and GlcNAc 6-OH in the β-D-Gal*p*-(1→4)-β-D-Glc*p*NAc-(1→ element was observed during the MD simulations of **9**. The NMR data show that modifications at Gal 6-C (Gal^{6d}/Gal^{6NH_2}) significantly affect the interaction between GlcNAc 3-OH and Gal 1-H, previously described.[22] Replacing the hydroxyl group by an amino group at Gal 6-C (**11**–**12**) deshields the Gal^{6NH_2} 3-OH and 4-OH signals, as well as the GlcNAc/GlcNPr 3-OH signal. ROEs between GlcNAc 3-OH and Gal^{6NH_2} 1-H could not be detected, which points either to some steric hindrance or to modification of the solvation shell originating from the Gal^{6NH_2} 6-NH group.

In general, the unusual $^3J_{OH,CH}$ coupling constants measured for GlcNAc 3-OH and Man 3-OH could be explained without the assumption of persistent hydrogen bonds. From MD simulations, the role of intramolecular hydrogen bonds has been described to be of minor importance in explicit solvent, as OH groups predominantly form hydrogen bonds to surrounding water molecules. These findings are in agreement with the results on methyl β-cellobioside,[4] where the interresidue 3-O–5-O hydrogen bond was reported to be insignificant in H_2O–CD_3OH. Using radial distribution functions, the analysis of the GlcNAc 3-OH solvation revealed a significant ordering of water molecules in the first solvation shell and the accessibility of the 3-OH group to the solvent. As a result, the OH groups are heavily involved in a relatively ordered network of water molecules covering the carbohydrate molecule surface, and form bridges which can extend across the glycosidic linkages (Fig. 9). A similar observation was recently reported for α-linked carbohydrates.[28]

To summarize, the upfield shifts of the GlcNAc 3-OH group are probably caused by the nearby ring and glycosidic O atoms as described for structures with a similar structural arrangement.[11–16] The shielding of Gal 4-OH when reducing the 2-C atom in **3** and **4** can only be attributed to a significant change in the water network covering the carbohydrate, since no direct interaction between 2-OH and 4-OH is possible. In addition, the large downfield shift introduced to some OH groups when introducing a NH_3^+ group at Gal 6-C (**11** and **12**) is likely to be caused by the positive charge, since the effect is only observed on adjacent groups and decreases with the distance.

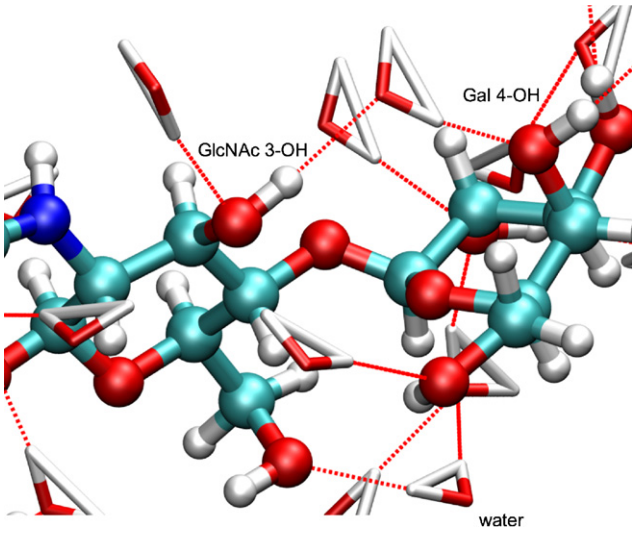

Figure 9. Snapshot of the hydrogen bonding network formed between water molecules, and Gal and GlcNAc residues of **1**.

4. Experimental

4.1. NMR measurements

The trisaccharides **1**–**12** have been synthesized previously.[24] Compounds were dissolved in 0.5 mL 85% H_2O/15% $(CD_3)_2CO$ to a final concentration of 25 mM for **2**, **4**, **5**, and **7**–**12**, and of 15, 20, and 20 mM for **1**, **3**, and **6**, respectively. For all compounds, the pH was adjusted to 7.05 ± 0.1 using 30 mM HCl, with the exception of **11** and **12** where the pH was set at 6.40 ± 0.05. In order to minimize the absorption of impurities from the glassware, NMR tubes were soaked for 24 h in 50 mM sodium phosphate, pH 7.[3] ^1H NMR spectra were generally recorded at 268 K on a BRUKER DRX-600 spectrometer, operating at 600.13 MHz for proton observation. For the determination of temperature coefficients, the temperature was lowered from 283 to 268 K in steps of 5 K, and from 268 K until the freezing point in steps of 1 K. One- and two-dimensional ^1H NMR spectra were acquired using the WATERGATE pulse sequence[29] for water suppression, and were calibrated by using acetone as internal standard ($\delta_H = 2.204$ ppm). The 2D DQF-COSY, TOCSY, NOESY, and ROESY spectra were acquired in the phase-sensitive mode using the state-TPPI method (time-proportional phase incrementation) with standard pulse sequences from the BRUKER

library. The rates of exchange of hydroxy protons with water were calculated from 2D NOESY/EXSY phase-sensitive chemical exchange experiments performed at 268 K. Mixing times of 3–21 ms in steps of 3 ms were used. The volumes of the signals stemming either from the NOEs or from the diagonals were measured using the program AURELIA (Bruker, Germany).

4.2. Molecular dynamics simulations

Molecular dynamics (MD) simulations of the oligosaccharides **1**, **3**, **9**, and **11** were realized in the nanosecond timescale. The AMBER* force field implemented in MacroModel 8.1 was used with standard parameters on isolated molecules for the gas phase and continuum solvent (GB/SA) model simulations.[30] MD simulations of **1** and the disaccharides β-D-Glc*p*NAc-(1→2)-α-D-Man*p*-OMe and 6-deoxy-β-D-Glc*p*NAc-(1→2)-α-D-Man*p*-OMe were performed in explicit solvent using periodic boundary conditions, the particle-mesh Ewald electrostatics, and the TIP3 water model. The *sander* module of the AMBER suite of programs[31] calculated the trajectories, and Tleap was used to connect the appropriate GLYCAM building blocks and build the starting structures.[32] The GLYCAM-04 parameters and charges were used for calculations on oligosaccharides. The 1–4 electrostatic (SCEE) and nonbonded (SCNB) scaling factors were set to unity as recommended by the developers. All MD simulations were performed at 300 K. Prior to sampling of snapshots, a two-step equilibration period was applied to the solvated system as follows. First the system was heated over a period of 20 ps from 10 to 300 K at constant volume, then the pressure and density of the water were adjusted during a 80 ps simulation period at constant temperature. The equilibration time for the simulations without explicit solvent was 10 ps. Simulations were performed over a production time of 30 ns (**1**) and 6 ns (**3**, **9**, **11**) for the gas phase/continuum solvent system and 10 ns when explicit solvent was present.

All trajectory data were analyzed using Conformational Analysis Tools (CAT).[33] Depending on the length of the simulation, 10,000–60,000 snapshots were implemented. To determine the possibility of hydrogen bonds, the following geometric criterions were employed: a H–A distance shorter than 2.5 Å and a D–H–A angle larger than 120°. Igor Pro (www.wavemetrics.com) generated the scientific plots.

Acknowledgements

This work was supported by the European Community Research Training Network Glycotrain (HPRN-CT-2000-00001).

References

1. Rivera-Sagredo, A.; Cañada, F. J.; Nieto, O.; Jiménez-Barbero, J.; Martín-Lomas, M. *Eur. J. Biochem.* **1992**, *209*, 415–422.
2. Solís, D.; Fernández, P.; Díaz-Mauriño, T.; Jiménez-Barbero, J.; Martín-Lomas, M. *Eur. J. Biochem.* **1993**, *214*, 677–683.
3. Adams, B.; Lerner, L. E. *J. Am. Chem. Soc.* **1992**, *114*, 4827–4829.
4. Leeflang, B. R.; Vliegenthart, J. F. G.; Kroon-Batenburg, L. M. J.; van Eijck, B. P.; Kroon, J. *Carbohydr. Res.* **1992**, *230*, 41–61.
5. Poppe, L.; van Halbeek, H. *J. Am. Chem. Soc.* **1992**, *114*, 1092–1094.
6. Sheng, S.; van Halbeek, H. *Biochem. Biophys. Res. Commun.* **1995**, *215*, 504–510.
7. Brisson, J.-R.; Uhrinova, S.; Woods, R. J.; van der Zwan, M.; Jarrell, H. C.; Paoletti, L. C.; Kasper, D. L.; Jennings, H. J. *Biochemistry* **1997**, *36*, 3278–3292.
8. Bekiroglu, S.; Kenne, L.; Sandström, C. *J. Org. Chem.* **2003**, *68*, 1671–1678.
9. Poppe, L.; van Halbeek, H. *J. Am. Chem. Soc.* **1991**, *113*, 363–365.
10. Poppe, L.; Stuike-Prill, R.; Meyer, B.; van Halbeek, H. *J. Biomol. NMR* **1992**, *2*, 109–136.
11. Sandström, C.; Baumann, H.; Kenne, L. *J. Chem. Soc., Perkin Trans. 2* **1998**, 809–815.
12. Sandström, C.; Baumann, H.; Kenne, L. *J. Chem. Soc., Perkin Trans. 2* **1998**, 2385–2393.
13. Bekiroglu, S.; Sandström, C.; Norberg, T.; Kenne, L. *Carbohydr. Res.* **2000**, *328*, 409–418.
14. Bekiroglu, S.; Kenne, L.; Sandström, C. *Carbohydr. Res.* **2004**, *339*, 2465–2468.
15. Bekiroglu, S.; Sandström, A.; Kenne, L.; Sandström, C. *Org. Biomol. Chem.* **2004**, *2*, 200–205.
16. Ivarsson, I.; Sandström, C.; Sandström, A.; Kenne, L. *J. Chem. Soc., Perkin Trans. 2* **2000**, 2147–2152.
17. Felemez, M.; Spiess, B. *J. Am. Chem. Soc.* **2003**, *125*, 7768–7769.
18. van Halbeek, H.; Poppe, L. *Magn. Reson. Chem.* **1992**, *30*, S74–S86.
19. Kindahl, L.; Sandström, C.; Norberg, T.; Kenne, L. *J. Carbohydr. Chem.* **2000**, *19*, 1291–1303.
20. Kindahl, L.; Sandström, C.; Norberg, T.; Kenne, L. *Carbohydr. Res.* **2001**, *336*, 319–323.
21. Harris, R.; Rutherford, T. J.; Milton, M. J.; Homans, S. W. *J. Biomol. NMR* **1997**, *9*, 47–54.
22. Poppe, L.; van Halbeek, H. *Struct. Biol.* **1994**, *1*, 215–216.
23. Rohfritsch, P. F.; Joosten, J. A. F.; Krzewinski-Recchi, M.-A.; Harduin-Lepers, A.; Laporte, B.; Juliant, S.; Cerutti, M.; Delannoy, P.; Vliegenthart, J. F. G.; Kamerling, J. P. *Biochim. Biophys. Acta* **2006**, *1760*, 685–692.
24. Joosten, J. A. F.; Evers, B.; van Summeren, R. P.; Kamerling, J. P.; Vliegenthart, J. F. G. *Eur. J. Org. Chem.* **2003**, 3569–3586.
25. Haasnoot, C. A. G.; de Leeuw, F. A. A. M.; Altona, C. *Tetrahedron* **1980**, *36*, 2783–2792.
26. Fraser, R. R.; Kaufman, M.; Morand, P.; Govil, G. *Can. J. Chem.* **1969**, *47*, 403–409.
27. Still, W. C.; Tempczyk, A.; Hawley, R. C.; Hendrickson, T. *J. Am. Chem. Soc.* **1990**, *112*, 6127–6129.
28. Almond, A. *Carbohydr. Res.* **2005**, *340*, 907–920.
29. Piotto, M.; Saudek, V.; Sklenár, V. *J. Biomol. NMR* **1992**, *2*, 661–665.

30. Mohamadi, F.; Richards, N. G. J.; Guida, W. C.; Liskamp, R.; Lipton, M.; Caufield, C.; Chang, G.; Hendrickson, T.; Still, W. C. *J. Comput. Chem.* **1990**, *11*, 440–467.
31. Case, D. A.; Cheatham, T. E., III; Darden, T.; Gohlke, H.; Luo, R.; Merz, K. M., Jr.; Onufriev, A.; Simmerling, C.; Wang, B.; Woods, R. J. *J. Comput. Chem.* **2005**, *26*, 1668–1688.
32. Woods, R. J.; Dwek, R. A.; Edge, C. J.; Fraser-Reid, B. *J. Phys. Chem.* **1995**, *99*, 3832–3846.
33. Frank, M., *Conformational Analysis Tools (CAT)*. http://www.md-simulations.de/CAT/.